Journal of Hazardous Materials Advances 18 (2025) 100657

Contents lists available at ScienceDirect

Journal of Hazardous Materials Advances

journal homepage: www.elsevier.com/locate/hazadv

Highly effective lead removal by novel alkaline biochar prepared by pyrolysis of woody biomass impregnated with low-level NaOH

Qiangu Yan [a,1], Neda Arabzadeh Nosratabad [b,1], Xiangwei Du [c], Timothy Ketelboeter [a], Caixia Wan [*,b], Zhiyong Cai [*,a]

[a] Forest Products Laboratory, USDA Forest Service, One Gifford Pinchot Drive, Madison, WI 53726-2398, USA
[b] Department of Chemical and Biomedical Engineering, University of Missouri, 1406 East Rollins Street, Columbia, MO 65211, USA
[c] Veterinary Medical Diagnostic Laboratory, University of Missouri, 901 E Campus Loop, Columbia, MO 65211, USA

ARTICLE INFO

Keywords:
Biomass
Alkaline biochar
Pyrolysis
Lead removal
Environmental remediation

ABSTRACT

The remediation of heavy metal-contaminated environments, particularly those polluted with lead, remains a critical challenge due to the metal's toxicity and persistence. This study developed a novel alkaline biochar for enhanced lead adsorption, prepared from pine wood through low-level NaOH (0–2 wt%) dry impregnation followed by pyrolysis at temperatures ranging from 350 to 600 °C. Characterization using scanning electron microscopy (SEM), X-ray diffraction (XRD), Fourier transform infrared spectroscopy (FTIR), and X-ray photoelectron spectroscopy (XPS) elucidated the alkaline biochar's surface modifications and adsorption mechanisms. Adsorption studies showed that 2 wt% NaOH-modified biochar (2 % NaOH-BC) achieved a maximum adsorption capacity of 230 mg g^{-1}, representing a 14-fold improvement over non-alkaline treated biochar (0 % NaOH-BC, 16.1 mg g^{-1}). Kinetic studies confirmed chemisorption as the dominant mechanism, described by the pseudo-second-order model, while Langmuir isotherm analysis (R^2 = 0.933–0.970) indicated monolayer adsorption. XPS analysis revealed the emergence of Pb^{2+} peaks after adsorption, indicating successful Pb^{2+} uptake. The analysis provided insights into the adsorption mechanism, suggesting ion exchange and coordination interactions involving oxygen-containing functional groups. Electrostatic interactions also played a role, as increasing pH (3.0–11.0) enhanced Pb^{2+} binding due to surface deprotonation, with optimal adsorption at pH 11.0 (266 mg g^{-1}, 100 % efficiency). These findings highlight the potential of low-cost NaOH-treated biochar for effective and sustainable lead remediation.

1. Introduction

Lead contamination in soils and waters has emerged as a pressing global concern due to its toxicity, persistence, and widespread distribution resulting from industrial processes, waste disposal, and agricultural activities (Monga et al., 2022; Zhou et al., 2017). Elevated lead levels pose serious environmental and public health risks, including bioaccumulation in ecosystems and neurological damage in humans (Omidvar-Hosseini and Moeinpour, 2016; Yang et al., 2019). Given the urgency of mitigating these hazards, a broad range of remediation strategies have been explored, including chemical precipitation, ion exchange, and adsorption-based methods (Fu and Wang, 2011). Among these, adsorption stands out for its high adsorption efficiency, rapid metal removal rate, eco-friendly nature, and ease of operation (Genç-Fuhrman et al., 2016; Lu et al., 2017; Xu et al., 2013). Developing low-cost adsorbents is key to practical implementation of adsorption techniques for environmental remediation from the economic perspective.

Biochar, a carbon-rich, low-density charred material derived from sustainable feedstocks pyrolysis, has proven to be a promising adsorbent for heavy metal remediation (Liu and Zhang, 2009; Wu et al., 2019). It offers several advantages over traditional adsorbents, such as activated carbon, including straightforward production methods, utilization of renewable feedstocks, and the presence of inherent functional groups capable of binding contaminants (Ippolito et al., 2020). However, pristine biochar often exhibits limited adsorption capacity due to relatively low surface area, inadequate porosity, and limited abundance of reactive functional groups (Amalina et al., 2024). To enhance biochar's

* Corresponding authors.
E-mail addresses: wanca@missouri.edu (C. Wan), zhiyong.cai@usda.gov (Z. Cai).
[1] These authors contributed equally.

https://doi.org/10.1016/j.hazadv.2025.100657
Received 24 September 2024; Received in revised form 2 February 2025; Accepted 20 February 2025
Available online 21 February 2025

surface characteristics and improve its adsorption efficiency, numerous modification strategies have been explored, such as physical activation, steam treatment, acidification, and alkaline treatment (Hagemann et al., 2018; Murtaza et al., 2024; Nosratabad et al., 2024; Ramola et al., 2022). The effectiveness of biochar can vary widely based on the type of feedstock used and the conditions under which it is produced, especially the pyrolysis temperature and any pre- or post-pyrolysis activation treatments (Amin et al., 2018; Bashir et al., 2018; Bentley et al., 2022; Chen et al., 2016; Chen et al., 2019; Ippolito et al., 2012; Lee and Shin, 2021; Mahdi et al., 2019; Nguyen et al., 2019; Rizwan et al., 2020; Shin et al., 2020; Wang et al., 2018; Wang and Wang, 2019; Zhao et al., 2022). Many studies have explored how pyrolysis temperatures and heating times influence the removal of contaminants, helping to improve treatment methods (Kwak et al., 2019). For example, Uchimiya et al. studied the effect of pyrolysis temperatures, 350 °C and 650 °C, on Pb^{2+} adsorption using broiler-litter-derived biochar. The results showed that biochar produced at the lower temperature was more effective at removing lead (Uchimiya et al., 2012). In contrast, other studies have demonstrated that higher pyrolysis temperatures can improve the adsorption efficiency of biochar for Pb^{2+} removal. For instance, cinnamon-derived biochar showed an increase in maximum adsorption capacity from 100.98 mg g^{-1} at 300 °C to 168.05 mg g^{-1} at 600 °C, attributed to enhanced surface characteristics and structural changes (Omidi et al., 2019). Furthermore, modification methods involving pre-treatment or post-treatment with acidic or basic solutions can alter the biochar's porous structure and modify the type and composition of its surface functional groups, thereby influencing its adsorption capacity (Jin et al., 2014; Liu et al., 2012). Among the alkaline reagents, KOH and NaOH are commonly used reagents for alkaline modification of biochar. NaOH modification offers several advantages over KOH modification, including a lower loading, reduced cost, greater environmental friendliness, and lower corrosivity (Cazetta et al., 2011). For example, NaOH-modified coconut biochar exhibited a substantial increase in surface area from 1940 to 2885 m^2 g^{-1}, outperforming KOH-modified coconut biochar (Cazetta et al., 2011; Tan et al., 2008). Despite enhanced biochar performance, alkaline treatment itself should be improved for cost-effectiveness and eco-friendliness. To this end, high-solid treatment with no/little generation of liquid waste can offer several benefits, including reducing usage of alkali, increasing biochar production capacity, lowering the production costs, and minimizing waste generation.

This study aimed to exploit facile, low cost dry impregnation for alkaline treatment of pine wood for production of alkaline biochar and to investigate the biochar's effectiveness in removing lead ion from aqueous systems. This approach involved applying a minimal amount of NaOH to pine with zero liquid waste prior to pyrolysis, making it less labor-/energy-intensive and more environmentally friendly than traditional alkaline treatment. The detailed adsorption isotherm and kinetics were also studied to evaluate lead removal capabilities of alkaline biochar and understand its adsorption mechanisms for lead ions. The work deomstrated a viable strategy for production of low-cost alkaline biochar and its use as an highly effective adsorbent for lead removal and environmental remediation.

2. Materials and methods

2.1. Biochar preparation

Pine particles furnish was used as the feedstock for biochar preparation. The alkaline treatment involved a dry impregnation process, where alkaline solutions with varying NaOH concentrations were mixed with the pine particles. The mixture was stirred continuously for 30 min, followed by intermittent stirring for 2 h. To ensure deeper penetration of the NaOH solution into the pine particles, a vacuum process was employed for 10 min. After impregnation in dark conditions for 24 h, the samples were air dried for 24 h, followed by oven drying at 105 °C for another 24 h, resulting in 0–2 wt% NaOH loadings in the dried samples (with the respective biochar samples labeled as 0 % NaOH-BC, 1 % NaOH-BC, and 2 % NaOH-BC). The treated feedstock was stored in air-tight containers.

The treated feedstock was further subjected to pyrolysis in a fixed-bed tubular reactor under a 99.99 % argon atmosphere, maintained at a flow rate of 0.2 SLPM for 30 min, with a heating rate of 20 °C/min. Pyrolysis temperature ranged from 350 to 600 °C.

The detailed proximate and elemental analysis of the pine particles are presented in **Table S1**. Activated carbon and other chemicals and reagents were purchased from Fisher Scientific (Hampton, NH), unless specified otherwise. A standard stock solution of lead nitrate ($Pb(NO_3)_2$) (0.05 M) was purchased from Reagents (Belmont, NC).

2.2. Characterization and analysis methods

The surface area of the alkaline biochars was determined using nitrogen adsorption isotherms (Micromeritics® TriStar II Plus, Norcross, GA, USA), employing the Brunauer–Emmett–Teller (BET) method for accurate measurement. The pH values of alkaline biochars were measured using a pH meter (BEP-M400B Benchtop pH/Ion Meter, Infitec Inc., Spokane, WA, USA). X-ray powder diffraction (XRD) patterns of the alkaline biochar samples were obtained using a Rigaku Ultima III X-ray Diffraction System (Rigaku, Woodlands, TX, USA). X-ray photoelectron spectroscopy (XPS) was carried out with a Thermo Scientific Nexsa PS system using a true monochromatic Al Kα X-ray source (72 W, 400 μm slot).Thermogravimetric analysis (TGA) was conducted using a Mettler Toledo TGA/DSC 3+ system (Mettler-Toledo, Columbus, OH, USA) to assess the thermal stability and decomposition behavior of the biochar samples. Inductively coupled plasma-optical emission spectrometry (ICP-OES) assessment was performed using the Thermo Scientific iCAP 7000 Plus Series. Lead was detected at 220.353 nm with a linear calibration range from 0.1 to 100 μg mL^{-1}. Furthermore, the characterization of functional groups present on the biochar surface were conducted using Fourier Transform Infrared Spectroscopy (Thermo Scientific, Nicolet iZ10). Additionally, Scanning Electron Microscopy (JEOL 6500F FE-SEM, Peabody, MA, USA) was utilized to examine the structure and morphology of the alkaline biochar samples. Elemental analysis was performed using an EDS system (XFlash 6–30, Bruker Nano GmbH, Berlin, Germany). Lastly, the iodine number, an indicator of the biochar's porosity, was determined in accordance with ASTM Standards D4607–94.

2.3. Adsorption experiments

In the sorption kinetics experiments, 75 mg of alkaline biochar was mixed with 250 mL of $Pb(NO_3)_2$ (70 ppm) solution in a 500 mL Erlenmeyer flask, and the experiment was conducted at ambient temperature (25 ± 2 °C). Subsequently, the solution was agitated at 300 rpm using a magnetic stirrer for up to 24 h to ensure equilibrium was reached. The samples were taken at a predetermined intervals and filtered (using a 0.45 μm nylon membrane filter) to collect the liquid for the determination of Pb^{2+} ions using ICP-OES. All experiments were performed in triplicate to ensure reproducibility.

The adsorption isotherm for lead removal was established following the same procedure described above, albeit with varying concentrations of Pb^{2+} (250 mL, 10–70 mg l^{-1}) in the sorbate suspensions.

The biochar's adsorption capacity and efficiency for Pb^{2+} ion was calculated following Eqs. (1) and (2), respectively:

$$q_e = \frac{(C_0 - C_e) \times V}{m} \tag{1}$$

$$Pb^{2+}\ \text{removal efficiency} = \left(\frac{C_0 - C_e}{C_0}\right) \times 100\% \tag{2}$$

Where C_0 (mg l^{-1}) is initial Pb^{2+} concentration, and C_e (mg l^{-1}) is Pb^{2+} concentration at equilibrium, V (L) is the volume of Pb^{2+}solution, m (g) is biochar mass, and q_e (mg g^{-1}) is the amount of adsorbed Pb^{2+} per unit mass of biochar.

The adsorption kinetics were studied using pseudo-first-order and pseudo-second-order kinetic models using Eqs. (3) and (4), respectively:

$$q_t = q_e\left(1 - e^{k_1 t}\right) \tag{3}$$

$$q_t = \frac{k_2\, q_e^2\, t}{(1 + k_2\, q_e\, t)} \tag{4}$$

where q_t and q_e (mg g^{-1}) are the adsorption capacity at time t (min) and at equilibrium, respectively, and k_1 (min^{-1}) and k_2 (g mg^{-1} min^{-1}) are the rate constants for pseudo-first-order and pseudo-second-order adsorption, respectively.

The adsorption isotherm was evaluated using the Langmuir and Freundlich models, expressed as follows:

$$Langmuir: q_e = \frac{q_m\, K_L\, C_e}{(1 + K_L\, C_e)} \tag{5}$$

$$Freundlich: q_e = K_{fr}\, C_e^{1/n_{fr}} \tag{6}$$

where q_m (mg g^{-1}) is the maximum adsorption capacity of the biochar, q_e (mg g^{-1}) is the equilibrium adsorption capacity, K_L (L mg^{-1}) is the Langmuir constant, and K_{fr} (mg g^{-1}) (mg $l^{-1})^{1/n}$ and $1/n_{fr}$ are the Freundlich constants.

2.4. Adsorption-desorption experiments

Seventy-five minigrams of 2 % NaOH-BC was combined with 250 mL of $Pb(NO_3)_2$ solution (70 ppm) and agitated until equilibrium was reached in the adsorption process. After equilibrium, the Pb^{2+}-loaded 2 % NaOH-BC was collected by vacuum filtration, washed with DI water 3–4 times, and dried at 80 °C for 5 h. Desorption experiments were then conducted by adding the dried Pb^{2+}-loaded 2 % NaOH-BC to 250 mL of desorption solution in an Erlenmeyer flask at room temperature (25 ± 2 °C). NaOH (0.1 M) was used as the desorption reagent to desorb Pb^{2+} from the 2 % NaOH-BC for 4 h to study the desorption behavior. The samples were taken at specific intervals, filtered through a 0.45 μm filter, and analyzed using ICP-OES. After desorption/regeneration, the biochar was collected using vacuum filtration, washed, and dried. The regenerated alkaline biochar was reused as the adsorbent in subsequent adsorption experiments. This process was repeated for four cycles to assess the recyclability of the adsorbents.

3. Results and discussion

3.1. Effect of pyrolysis parameters on alkaline biochar production

Fig. 1a depicts the yields of biochar obtained at pyrolysis temperatures ranging from 350 to 650 °C, with NaOH loadings ranging from 0 to 2 wt%. At the lower temperature of 350 °C, the biochar yields are generally higher compared to those at 650 °C across all the NaOH loadings. This observation suggests that the pyrolysis at 350 °C, potentially in conjunction with the catalytic effects of NaOH, is more conducive to yielding a greater quantity of biochar. As the NaOH concentration increases, there is a discernible improvement in biochar yield, indicating that NaOH plays a role in the carbonization process, potentially by enhancing the decomposition of lignocellulosic structures into char. Fig. 1b presents the relationship between NaOH loading and the alkalinity/pH of biochar produced at a constant pyrolysis temperature of 550 °C under an argon atmosphere for 0.5 hr. The pH of the biochar significantly increased with the NaOH content, starting from a pH value of ~7 for the 0 % NaOH-BC and reaching a much higher pH value of ~12.8 for 2 % NaOH-BC. The sharp rise of pH when increasing the NaOH loading from 0 % to 0.5 % indicated a substantial impact of even small amounts of NaOH, likely due to the introduction of basic functional groups and inorganics during the pyrolysis process. These findings agree with the TGA analysis.

Effects of pyrolysis temperature on the biochar yields and its pH values were studied on 0 to 2 wt% NaOH-pine under an argon atmosphere for 30 min (**Figure S1a**). The results indicated a clear trend of decreasing alkaline biochar yield when the pyrolysis temperature increased. The reduction in alkaline biochar yield at elevated pyrolysis temperatures may be attributed to the volatilization of organic matters (Tomczyk et al., 2020). Nevertheless, the biochar yield of the 2 % NaOH-treated wood is consistently higher than that of the other NaOH loadings across all the temperatures. This suggests that the addition of NaOH contributed to more efficient carbonization catalyzed by alkali during pyrolysis. It should be noted that elevating temperature also led to a higher pH value of 2 % NaOH-BC (**Figure S1b**). This could be attributed to the formation of more inorganic minerals/alkaline compounds, which suggests that the biochar has a high cation exchange capacity and pH-buffering capacity (Chandraiah, 2016).

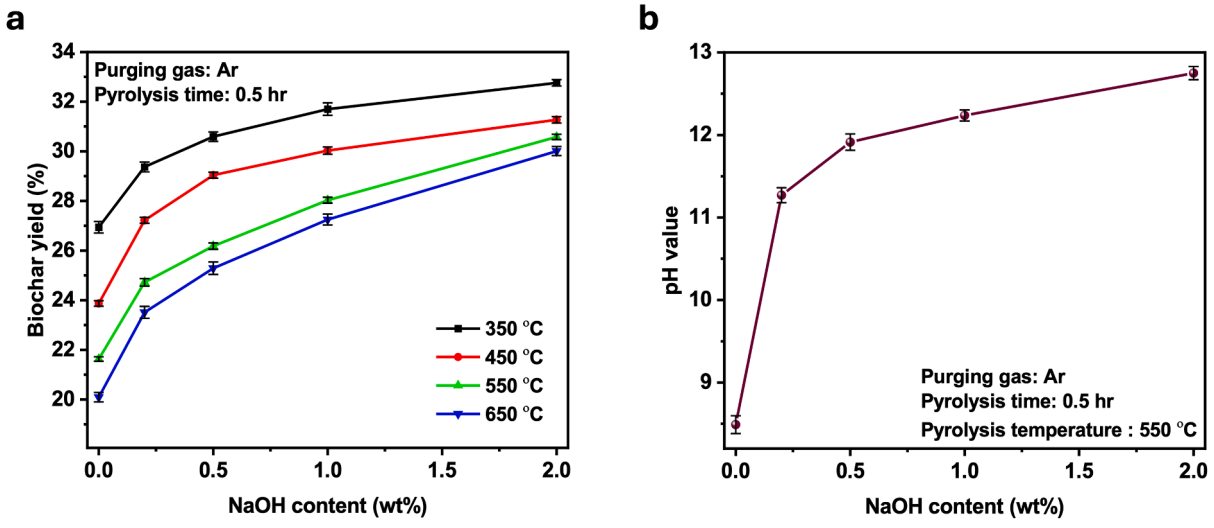

Fig. 1. (**a**) Effects of NaOH loading on biochar yield at different pyrolysis temperatures (350-650 °C, (**b**) Effects of alkaline loading on biochar pH values.

3.2. Alkaline biochar characteristics

3.2.1. Chemical change of pine wood by alkaline treatment

The FTIR spectra revealed distinct absorption bands of wood's chemical structure (**Figure S2 and Table S2**). The spectrum of untreated pine displays prominent peaks indicative of hydroxyl groups at 3331.1 cm^{-1}, methylene stretching at 2926.0 cm^{-1}, and methyl groups at 1453.3 cm^{-1}, which are typical of cellulose and hemicellulose structures. A reduction in the peak intensity of the hydroxyl group (3331.1 cm^{-1}) suggests the deprotonation and breaking of hydrogen bonds as NaOH concentration increased. There is also a noticeable decrease in the intensity of the peaks associated with lignin and hemicelluloses, such as those at 1423.8 cm^{-1}, which are associated with the scissoring of CH_2 and CH_3 in lignin, and 1265.9 cm^{-1}, which is attributed to C—O stretching in lignin and hemicellulose. These alterations are indicative of chemical modification of pine by NaOH, which subsequently determined biochar adsorptive capacities.

3.2.2. Thermal properties

Pine samples were also analyzed for key thermophysical properties. Characteristically, the principal peak in the derivative thermogravimetric (DTG) curves is associated with the thermal decomposition of cellulose. This peak is usually preceded by an earlier, less intense peak signifying hemicellulose breakdown, and followed by a persistent, elevated baseline towards higher temperatures, indicative of the more gradual degradation of lignin (Carrier et al., 2011). The weight loss depicted in Fig. 2a and b can be categorized into three distinct phases: an initial dehydration phase (approximately 50–150 °C), a primary active pyrolysis phase (200–400 °C), and a final passive pyrolysis phase (400–600 °C). In the first phase, the minimal mass reduction was due to the evaporation of water and light volatile substances, particularly noted in the NaOH-treated biochar samples. The second phase exhibited significant mass loss, predominantly due to the breakdown of hemicellulose, cellulose, and lignin, which agrees with the typical pyrolysis behavior of lignocellulosic materials (W.-J. Liu et al., 2017). The TG curves for the NaOH-modified biochar samples showed two distinct steps of mass loss (Fig. 2a). The wood decomposition temperatures decreased with increasing NaOH contents (i.e., 0 % NaOH-BC with 0.91 %/ °C at 359 °C vs. 2 % NaOH-BC with 0.68 %/ °C at 301 °C) (Fig. 2b), indicating that NaOH promoted the breakdown of the chemical bonds in wood. NaOH acted as a catalyst, cleaving interunit bonds between hemicellulose, cellulose, and lignin. During this active pyrolysis phase, the gradual release of organic constituents led to a significant decrease in mass and the generation of primary pyrolysis products. In the third phase, the remaining carbon-rich material continued to decompose at a lower rate across a broad temperature range (Carrier et al., 2011). It should also be noted that the biochar yields at 600 °C increased with NaOH level, reaching a maximum of 31.9 % at 2.0 % NaOH, about 20 % higher than that of the untreated biochar (Fig. 2a). The differential scanning calorimetry (DSC) curves, which indicate the heat flow associated with the wood's thermal events, show that the addition of NaOH altered both endothermic and exothermic reactions, as evidenced by variations in the intensity and position of the peaks (Fig. 2**c**). Notably, there is a significant negative peak for the blank samples between 300 and 400 °C, indicating that the pyrolysis of the original wood sample was an endothermic process. In contrast, there are exothermic (positive) peaks for the NaOH-wood samples, which became stronger and shift to lower temperatures with increasing NaOH content. These exothermic peaks, associated with decomposition reactions, became more profound with increased NaOH content, potentially indicating the formation of bonds between functional groups (such as hydroxyl) in the wood and sodium ions (Na^+). Sodium ions can partially replace protons in hydroxyl groups, forming structures similar to sodium carboxymethyl cellulose (Na-CMC), which usually decomposes at about 270 °C (Sugama and Pyatina, 2015).

3.2.3. XRD patterns

The XRD patterns reveal the crystalline structures of alkaline biochar, with distinct peaks associated with specific mineral phases (Fig. 3**a**). The alkaline biochar showed multiple peaks, ranging from ~27° to 40°, suggesting the presence of mineral crystals such as SiO_2 (silica), $CaCO_3$ (calcite), and Na_4SiO_4 in the biochar matrix (Jianghong Zhang et al., 2018). NaOH treatment led to significant alterations in peak intensity and position, suggesting an increase in the crystallinity of specific mineral phases or the formation of new Na-based minerals. At the highest loading of 2 %, the pattern suggests both the formation of new peaks and the disappearance or reduction of others. It is worth noting the presence of a broad peak (002) at around 20–30°, which is typically associated with the amorphous region with a high carbon content structure in biochar. Such biochar has turbostratic carbon, characterized by disordered graphitic crystallites (Keiluweit et al., 2010; L. Lu et al., 2002). Similar to NaOH level, pyrolysis temperature also exhibited significant effects on crystalline structures of biochar (**Figure S3a**). As the temperature increases, there is a noticeable evolution in crystalline patterns, especially associated with the formation of new Na-based minerals. This broadening peak in the 20°−30° range indicates the effective disintegration of the biomass structure at pyrolysis temperatures above 300 °C, aligning with TG analysis (Gupta et al., 2016; Keiluweit et al., 2010).

3.2.4. Morphology and microstructure

The surface morphologies of alkaline biochars were revealed by SEM images (Fig. 3**b**). Alkaline treatment led to roughing in biochar surface and the degree of roughness increased with NaOH level. Compared to relatively smooth surface of 0 % NaOH-BC (Fig. 3**b (i)**), the biochar with the higher NaOH levels (1–2 %) (Fig. 3**b** and **Figure S3b (i) to (iii)**)

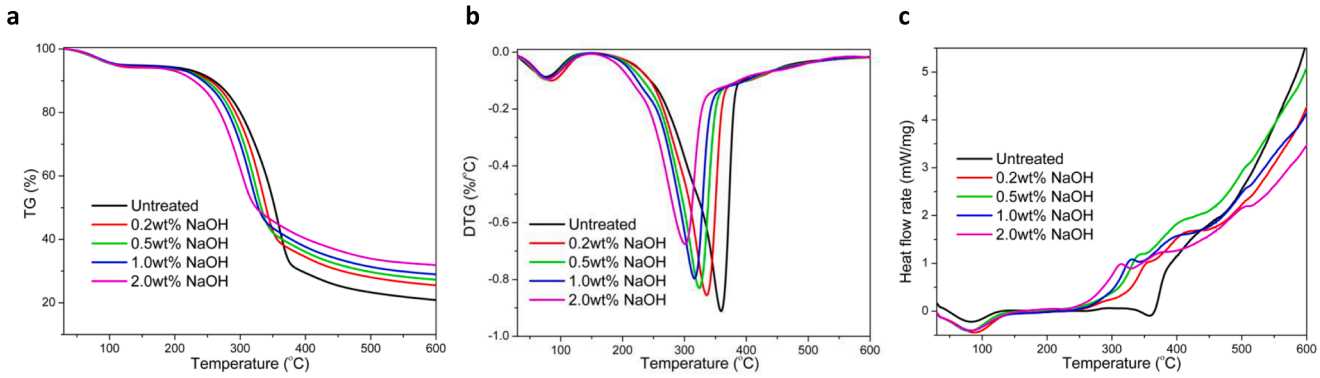

Fig. 2. Effects of alkaline loading on the thermal properties of biochar: (**a**) Thermogravimetric, (**b**) Derivative thermogravimetric, and (**c**) Differential scanning calorimetry.

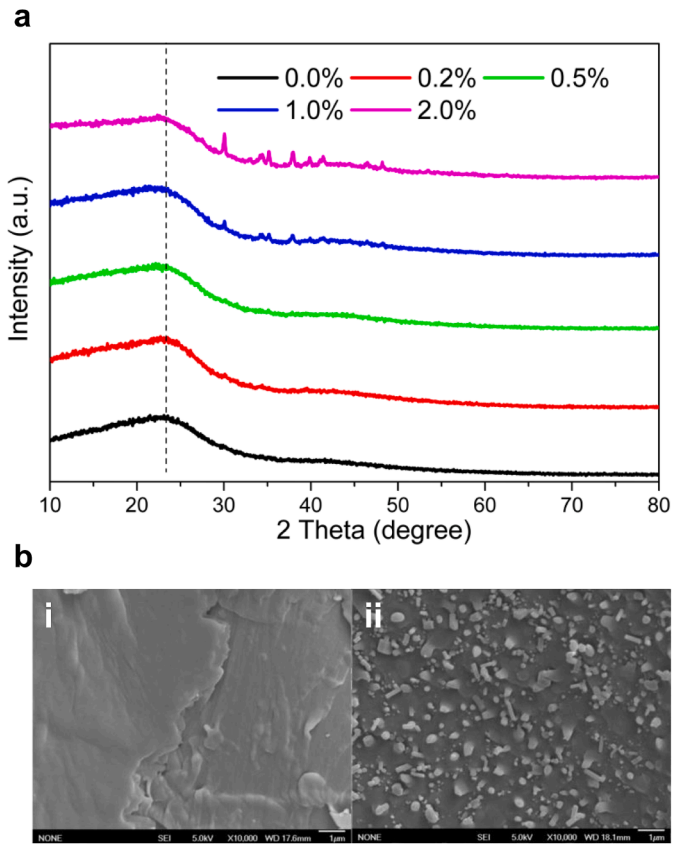

Fig. 3. (**a**) XRD patterns of biochar obtained from pyrolysis of NaOH-treated pine at 550 °C. (**b**) SEM images of NaOH-modified biochar: (i) 0 % NaOH-BC, and (ii) 2 % NaOH-BC. These NaOH-BCs samples were prepared at the pyrolysis temperature of 550 °C.

revealed more pronounced surface changes due to etches, pits, and/or the formation of new particulate matters. In the case of 2 % NaOH-BC (Fig. 3**b (ii)**), it even showed high density of pores or even layered appearance, suggesting a more aggressive interaction between NaOH and the biochar. Like other characteristics, elevating pyrolysis temperature to higher levels (550 °C and above) led to substantially modified surface with more pores or fissures and more uniform pore size distribution due to intense thermal decomposition (**Figure S4**), which confirmed porosity and TA analysis. The alkaline biochar obtained at 600 °C showed a highly evolved char structure with well-developed pores and potentially graphitic domains, indicative of high degree of carbonization. The observed trends provide insights into the porosity development, which is a critical characteristic for the application of biochar in mineral adsorption and soil amendments.

The adsorption capacity of biochar is significantly influenced by its surface area and porosity (Li et al., 2017). While increasing the alkaline level through NaOH treatment may not directly increase the BET surface area or pore volume due to the partial blocking of micropores by residual Na_2CO_3 particles, it does enhance average pore diameters (Table 1). The slight reduction in BET surface areas and pore volumes with increasing NaOH content in the alkaline biochar samples can be attributed to the partial blockage or filling of micropores by Na_2CO_3 particles formed during the alkaline treatment. However, when the NaOH-modified biochar samples are purified to remove Na_2CO_3, their BET surface areas and total pore volumes increase significantly. For instance, 2 % NaOH-BC, after being washed with hot DI water five times to eliminate sodium, exhibited a surface area of 536 m^2/g and a pore volume of 0.1209 $cm^3\ g^{-1}$. Nevertheless, even without purification, the 2 % NaOH-BC exhibited a high surface area of 248.001 $m^2\ g^{-1}$, an average pore diameter of 11.105 Å, and a porosity of 0.0689 $cm^3\ g^{-1}$, which are

Table 1
BET surface area, average pore diameter, and total pore volume of alkaline biochar samples.

Alkaline Biochar	BET Surface Area ($m^2\ g^{-1}$)	Average pore diameter (Å)	Pore Volume ($cm^3\ g^{-1}$)
0 % NaOH-BC	288.067	10.600	0.0763
0.2 % NaOH-BC	276.089	10.938	0.0755
0.5 % NaOH-BC	271.021	10.786	0.0731
1 % NaOH-BC	240.802	11.007	0.0702
2 % NaOH-BC	248.001	11.105	0.0689

higher than those reported for several other biochars in prior studies (Liu et al., 2022; Wang and Wang, 2019). In contrast, pyrolysis temperature had a more noticeable impact on the porosity and surface area of alkaline biochars. As shown in **Table S3**, increasing the pyrolysis temperature led to a clear improvement in porosity. Interestingly, the increase in surface area appears to result from the formation of new pore structures rather than the expansion of existing ones since the average pore diamters remained relatively unchanged. Similarly, the pore volume also increased, suggesting higher temperatures promote the development of additional pores. These improvements enhance the alkaline biochar's adsorption potential, making it more effective for environmental remediation applications.

3.3. Adsorption of lead ion onto NaOH-modified biochar

3.3.1. Adsorption kinetics and efficiency

The adsorption behavior of Pb^{2+} was analyzed using non-linear fitting of two different kinetic models: pseudo-first-order and pseudo-second-order, which assume adsorption rate control primarily by adsorbate diffusion and chemical adsorption, respectively. Pb^{2+} adsorption onto alkaline biochars (0 %, 1 % and 2 % NaOH-BC) proceeded through an initial fast adsorption phase within the first 30 min, followed by a slower phase at a steady rate until equilibrium was reached at around 1 h (Fig. 4**a** and **b**). This trend suggests a two-step adsorption mechanism: initially, a rapid adsorption phase driven by surface affinity, followed by a slower intraparticle diffusion phase, where Pb^{2+} ions penetrated deeper into internal pores structures (Mohan et al., 2014). Based on the data in Table 2, the pseudo-second-order model provided a better fit with higher correlation coefficient (R^2) values than the pseudo-first-order model, indicating that Pb^{2+} adsorption onto NaOH-modified biochars was primarily controlled by chemisorption rather than simple diffusion. This process was governed by specific interactions between the Pb^{2+} ions and functional groups on the biochar surface, involving electron sharing or exchange, thereby forming bonds through valence forces (Yari et al., 2015). This mechanism explained the strong affinity of Pb^{2+} ions to the adsorbent's surface.

As NaOH loading increased, the adsorption capacity improved, as reflected in the higher rate constants (k_1 and k_2) for 2 % NaOH-BC compared to 0 % NaOH-BC. This indicates that increasing NaOH loading for pine treatment led to enhanced Pb^{2+} adsorption by improving the availability of binding sites, increasing surface functionalization, and facilitating ion exchange. Additionally, the alkaline treatment enhanced the material's ion exchange capacity, playing a significant role in Pb^{2+} removal. The presence of NaOH likely increased the density of negatively charged sites, allowing stronger electrostatic interactions with Pb^{2+}. This is consistent with the observed trend that higher NaOH-modified biochar exhibited greater Pb^{2+} uptake, suggesting that Pb^{2+} removal was enhanced not only by an improved surface area but also by efficient cation exchange with Na^+.

Fig. 6**a** illustrates the adsorption performance of 0 %, 1 %, and 2 % NaOH-modified biochars over varying contact times. The 2 % NaOH-BC rapidly reached equilibrium, demonstrating its high efficiency in

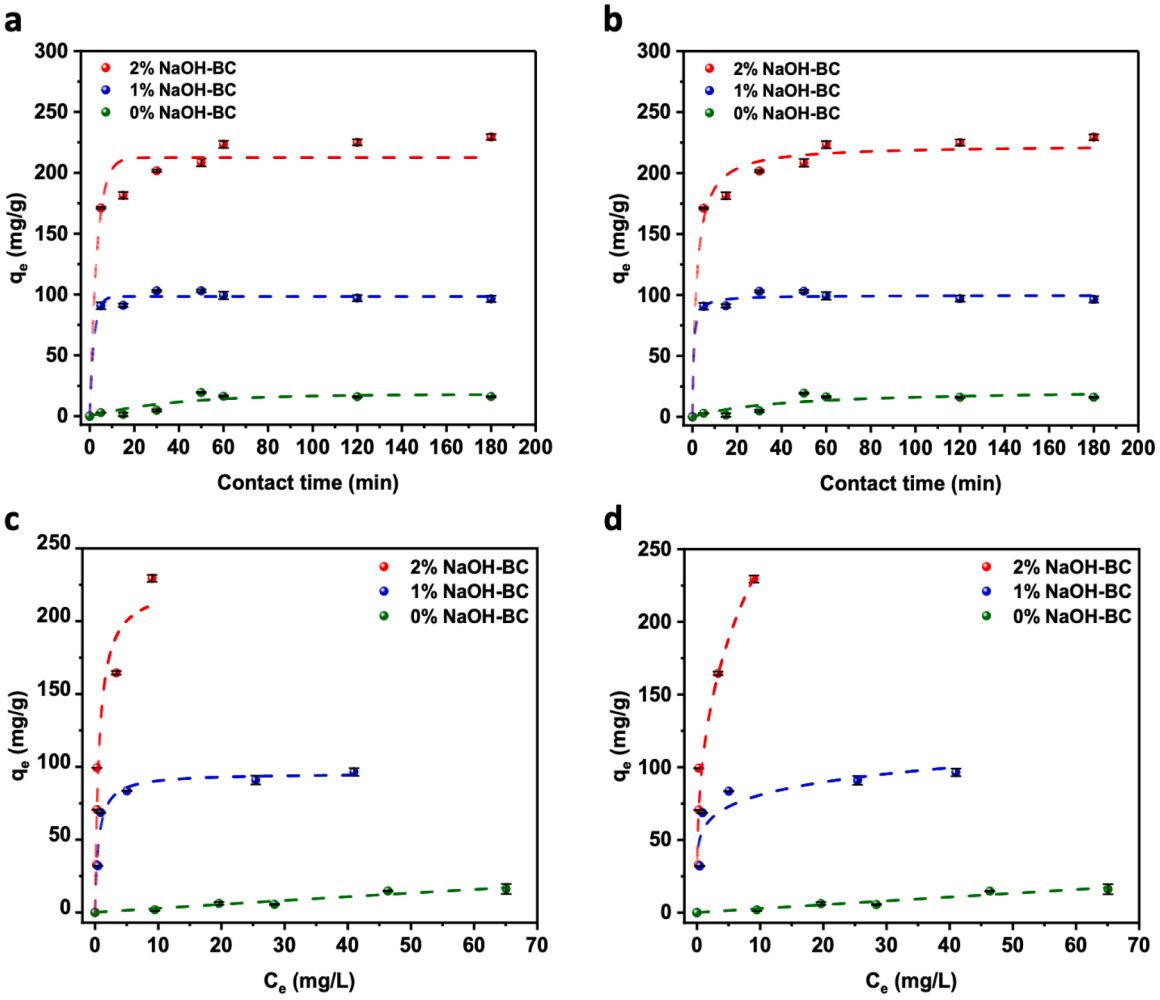

Fig. 4. Kinetics and isotherm models of 0 %, 1 % and 2 % NaOH-BC in Pb^{2+} removal: (**a**) Pseudo-first-order, (**b**) Pseudo-second-order, (**c**) Langmuir, and (**d**) Freundlich models.
Experimental conditions: adsorbent loading, 0.3 g l^{-1}; $Pb(NO_3)_2$ solution, 70 mg l^{-1}. For isotherm experiments, $Pb(NO_3)_2$ concentrations ranged from 10 to 70 mg l^{-1}.

capturing Pb^{2+} ions. In contrast, biochars with lower NaOH loadings showed reduced performance, with 1 % NaOH-BC achieving a capacity of 96.4 mg g^{-1} and 0 % NaOH-BC displaying negligible removal efficiency and a capacity of only 16.1 mg g^{-1}. These results highlight the enhanced adsorption capacity of 2 % NaOH-BC, emphasizing its potential as a cost-effective and efficient adsorbent for Pb^{2+} removal in environmental remediation.

3.3.2. *Adsorption isotherm studies*

Adsorption isotherms show how adsorbate molecules distribute between the liquid and solid phases once equilibrium is reached. Fitting the data to different models helps determine the best way to describe the adsorption process (Hameed et al., 2008). To optimize the adsorption system design for NaOH-modified biochars, the equilibrium data were analyzed using two nonlinear adsorption isotherm models, Langmuir and Freundlich, as shown in Fig. 4**c** and **d**. The Langmuir and Freundlich isotherm models, each characterized by two parameters, provide valuable information on adsorption capacity and constants associated with activation energy (Vijayaraghavan et al., 2006). Table 3 presents the maximum adsorption capacity (q_m), R^2, and other model constants obtained from the experimental data.

The Langmuir model describes adsorption as a process occurring on an ideal surface with energetically equivalent sites, where molecules form a monolayer coverage on the adsorbent, filling available sites and

Table 2
Pseudo-first-order and pseudo-second-order model parameters.

Alkaline Biochar	$q_{e,exp}$ (mg g^{-1})	Pseudo-first-order			Pseudo-second-order		
		q_e (mg g^{-1})	k_1 (min^{-1})	R^2	q_e (mg g^{-1})	k_2 (g mg^{-1} min^{-1})	R^2
2 % NaOH-BC	230.0	212.46	0.3092	0.961	223.0	0.0024	0.984
1 % NaOH-BC	96.42	98.32	0.5089	0.988	99.70	0.0188	0.990
0 % NaOH-BC	16.10	17.81	0.0262	0.795	22.76	0.0010	0.762

Table 3
Langmuir and Freundlich parameters for Pb^{2+} adsorption onto alkaline biochars.

Alkaline Biochar	Langmuir			Freundlich		
	q_m (mg g^{-1})	K_L (L mg^{-1})	R^2	K_{fr} (mg g^{-1}) (mg $l^{-1})^{1/n}$	n_{fr}	R^2
2 % NaOH-BC	226.20	1.54	0.933	108.0	0.345	0.926
1 % NaOH-BC	95.58	1.74	0.970	57.14	0.150	0.764
0 % NaOH-BC	41.14	1.60	0.943	0.280	0.986	0.918

preventing further migration of adsorbates molecules in the surface plane (Langmuir, 1918). According to Table 3, the q_m values obtained from the Langmuir isotherm were 226.2 mg g^{-1} for 2 % NaOH-BC (R^2 = 0.933), 95.58 mg g^{-1} for 1 % NaOH-BC (R^2 = 0.970), and 41.14 mg g^{-1} for 0 % NaOH-BC (R^2 = 0.943). These q_m values extracted from the model closely align with the experimental values, such as 230 mg g^{-1} for 2 % NaOH-BC and 96.42 mg g^{-1} for 1 % NaOH-BC. The separation factor (R_L), introduced by Weber and Chakkravorti, is a key parameter for characterizing the Langmuir isotherm (Weber and Chakravorti, 1974). The value of R_L determines the nature of adsorption: it indicates irreversible if $R_L = 0$, favorable if $0 < R_L < 1$, linear if $R_L = 1$, and unfavorable if $R_L > 1$. The R_L values for the NaOH-modified biochars all fell within the range of 0 to 1, confirming that Pb^{2+} adsorption onto these biochars is favorable (Amosa, 2016).

The Freundlich model is an empirical equation that describes adsorption on a heterogeneous surface, where adsorption initially occurs at the most energetically favorable sites (Freundlich, 1907). As these high-affinity sites become occupied, the binding strength gradually decreases with increasing surface coverage. The heterogeneity factor (n_{fr}) provides insight into the nature of the adsorption process, where $n_{fr} = 1$ suggests a linear, $n_{fr} < 1$ indicates chemical, and $n_{fr} < 1$ corresponds to physical adsorption (Cazetta et al., 2011; Fytianos et al., 2000). Based on the results in Table 3, the n_F value of 0.345 for 2 % NaOH-BC (R^2 = 0.926), 0.150 for 1 % NaOH-BC (R^2 = 0.764), and 0.986 for 0 % NaOH-BC (R^2 = 0.918) confirm that the adsorption process is predominantly chemical in nature.

By comparing the R^2 values (Table 3), it is evident that the Langmuir model provides the best fit, exhibiting the highest R^2 value. This suggests that Pb^{2+} ions were adsorbed as a monolayer on specific adsorption sites of the NaOH-modified biochars.

3.3.3. *SEM-EDS analysis of Pb^{2+} adsorption*

Fig. 5 depicts the structure and chemical composition of 2 % NaOH-BC before and after Pb^{2+} adsorption, captured through SEM and EDS elemental mapping. Before adsorption (Fig. 5**a**), the biochar surface appeared rough and porous. The corresponding EDS mapping showed no detectable Pb^{2+} signals (Fig.5c and its inset),the biochaeared rough and porous. The corresponding EDS mapping (Fig. 5c and its inset) showed no detectablePb^{2+} signals, confirming the absence of Pb^{2+} on the surface . In contrast, after Pb^{2+} adsorption (Fig. 5**b**), the alkaline biochar surface appeared clustered, with pores occupied by Pb^{2+} ions. EDS mapping in panel **d** further validated this, with the inset showing Pb^{2+} distribution as orange-coded areas. The presence of Pb^{2+} in panel **d**, compared to its absence in panel **c**, provides a strong evidence of effective Pb^{2+} ion adsorption by 2 % NaOH-BC.

Additionally, backscattered electron detector (BSED) SEM images of 2 % NaOH-BC before and after Pb^{2+} adsorption (**Figure S5**) further support these findings. The distinct bright spots in the post-adsorption image (**Figure S5b**) indicate Pb^{2+} adsorption, in contrast to the pre-adsorption image (**Figure S5a**), where no bright spots are visible. This is attributed to Pb's high atomic number, generating a stronger backscattering signal than lighter elements like carbon, making Pb-containing areas appear brighter in BSED images. Overall, these results confirm the effective Pb^{2+} adsorption by 2 % NaOH-BC, as demonstrated by SEM-EDS analysis.

3.3.4. *Effect of solution pH on biochar adsorption*

The pH of the solution plays a crucial role in the adsorption process, as it influences the surface charge of the adsorbent and the ionization degree of the heavy metal ions being adsorbed (Al-Ghouti et al., 2010; Ding et al., 2016; O'Connell et al., 2008). To evaluate its impact on Pb^{2+} adsorption, experiments were conducted at the pH levels of 3.0, 7.0, and 11.0 using 2 % NaOH-BC. As illustrated in Fig. 6**b**, the adsorption capacity and efficiency of Pb^{2+} improved with increase of pH from 3.0 to 11.0. At low pH, protonation of the hydrated surface of 2 % NaOH-BC's results in a positive charge. Additionally, excess H^+ ions compete with Pb^{2+} ions for the available adsorption sites on the 2 % NaOH-BC (Cai et al., 2021; Zahedifar et al., 2021). This competition, combined with the strong electrostatic repulsion between the positively charged 2 % NaOH-BC surface and cationic Pb^{2+} ions, reduces adsorption at pH 3.0.

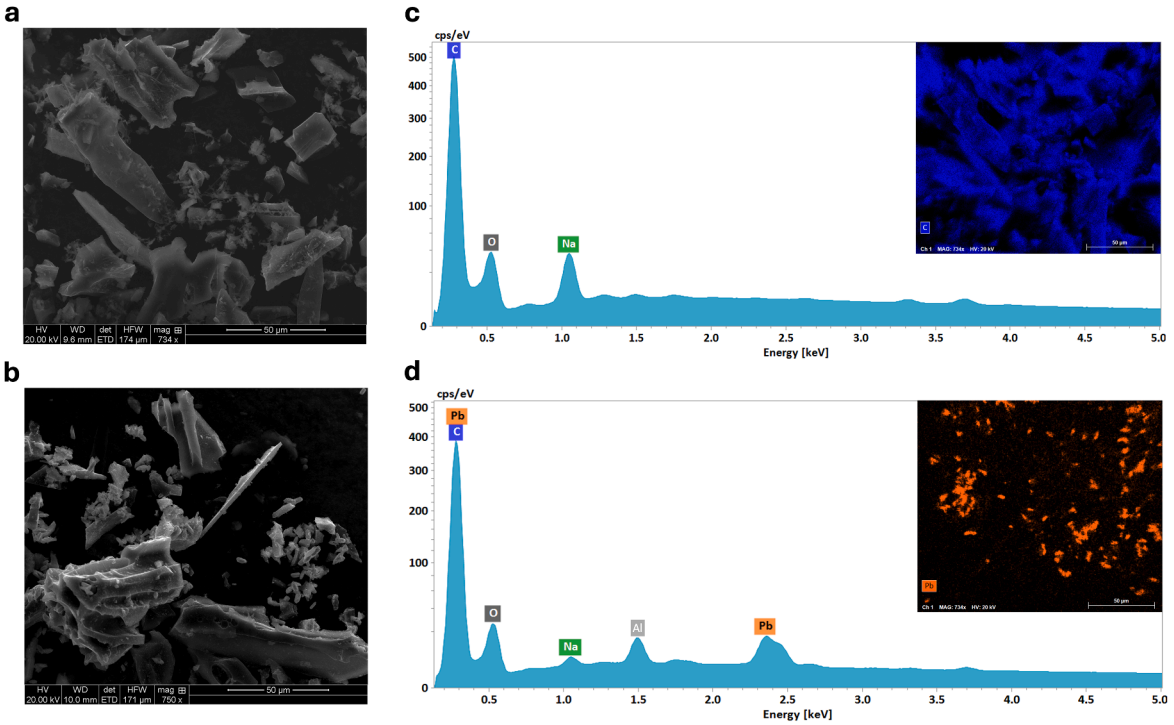

Fig. 5. SEM images and EDS elemental mapping analysis of 2 % NaOH-BC: (**a, c**) before, and (**b, d**) after Pb^{2+} adsorption. Insets in panels **c** and **d** show elemental distributions (carbon in blue, Pb^{2+} ions in orange).

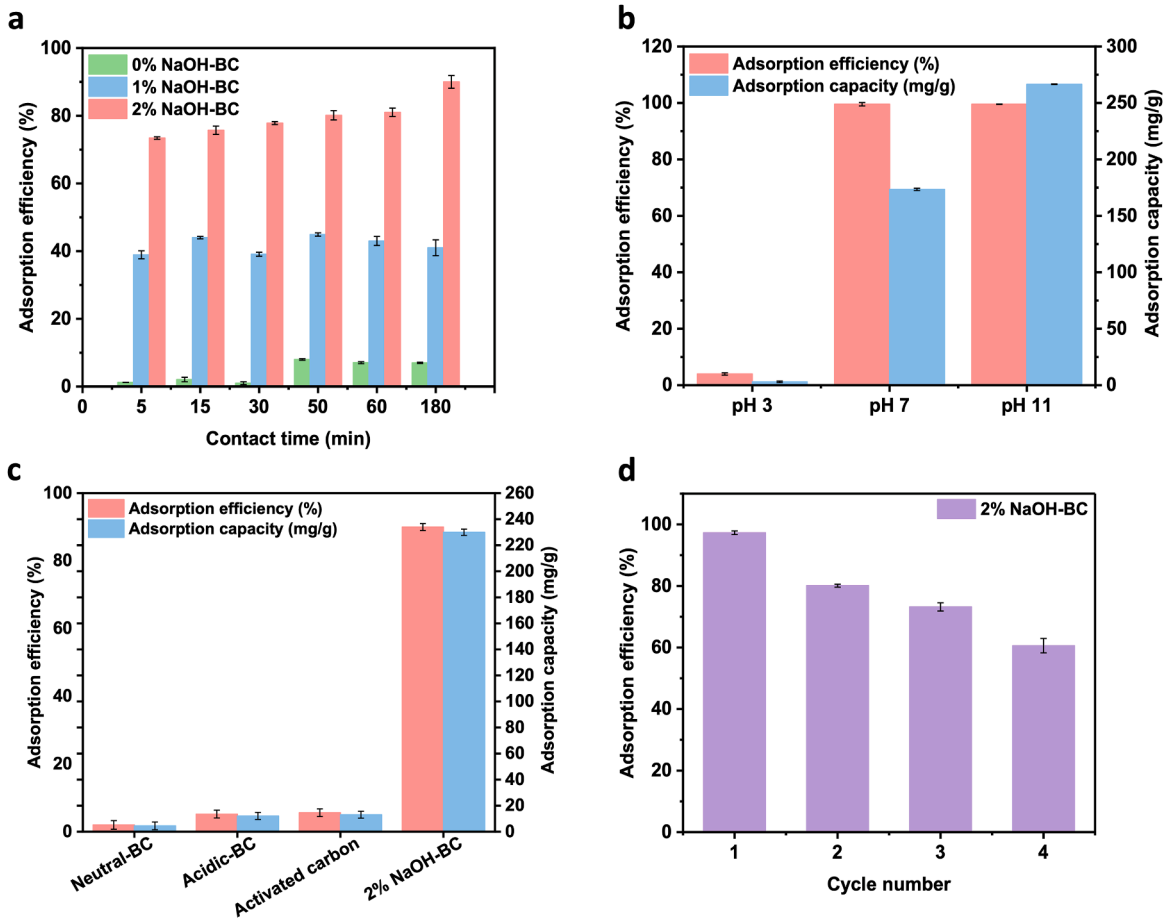

Fig. 6. (**a**) Adsorption performance of NaOH-BC with varying NaOH loadings (0 %, 1 %, and 2 %) over time for Pb^{2+} removal, (**b**) Effect of the solution pH on Pb^{2+} adsorption, and (**c**) Comparison of Pb^{2+} ion adsorption capacities and efficiencies among 2 % NaOH-BC, neutral-BC, acidic-BC, and activated carbon, (**d**) Reusability of 2 % NaOH-BC during Pb^{2+} ions adsorption.
Experimental conditions: 2 % NaOH-BC or activated carbon loadings: 75 mg; $Pb(NO_3)_2$ solution: 70 mg l^{-1}.

However, as the pH increases, deprotonation of functional groups on the 2 % NaOH-BC's hydrated surface generates more negatively charged sites (Li et al., 2017; Namazian and Halvani, 2006; Yap et al., 2017). This enhances the electrostatic attraction between the 2 % NaOH-BC's and Pb^{2+} ions, ultimately increasing the adsorption performance.

The influence of the inherent pH of the 2 % NaOH-BC itself on adsorption performance was also studied. As shown in Fig. 6**c**, the 2 % NaOH-BC (highly alkaline) exhibited the highest adsorption capacity, significantly outperforming its acidic and neutral counterparts. The weaker performance of acidic and neutral 2 % NaOH-BC can be attributed to the limited availability of negatively charged functional groups. In acidic 2 % NaOH-BC, protonation of carboxyl groups (-COOH) reduces the number of negatively charged sites, while neutral 2 % NaOH-BC lacks sufficient alkalinity to enhance Pb^{2+} binding. In contrast, the high surface alkalinity of 2 % NaOH-BC provides abundant negatively charged sites, enabling stronger electrostatic attraction and ion exchange with Pb^{2+} ions.

Compared to most biochars especially wood-based reported in prior studies (**Table S4**), 2 % NaOH-BC had a much higher adsorption capacity (230 mg g^{-1}). It even showed more than tenfold higher adsorption capacity than activated carbon (13 mg g^{-1}) (Fig. 6**c**). It should be noted that botanical origins with distinct chemical compositions and structural properties can influence the adsorption characteristics of derived biochar samples. This may explain why NaOH-BC did not outperform some non-woody biochars, such as camellia shells-based biochar although it had higher surface area and pore volumes (Ahmad et al., 2018; Cai et al., 2021). Nevertheless, the alkaline biochar especially 2 % NaOH-BC had favorable attributes, including abundant oxygen-containing functional groups (e.g., carboxyl, hydroxyl), enhanced ion exchange capacity, and high surface alkalinity, all contributing to its outstanding Pb^{2+} adsorption performance.

3.3.5. *Adsorption-desorption studies*

The stability and reusability of adsorbents during the adsorption–desorption process are crucial for ensuring the cost efficiency of the adsorption method. These studies are essential for reducing environmental remediation costs by identifying adsorbents suitable for long-term use at a larger scale. Therefore, the regeneration and reusability of the alkaline biochar was examined and the adsorption experiment was done four times under optimal conditions (pH = 6, initial Pb^{2+} ion concentration = 70 ppm, adsorbent loading = 0.3 g L^{-1}, contact time = 4 h). The reusability of 2 % NaOH-BC is depicted in Fig. 6**d**, in which as the number of adsorption–desorption cycles increased, the adsorption efficiency of 2 % NaOH-BC for Pb^{2+}dropped from 97.3 % in the first cycle to 80.1 % in the second cycle. It further decreased to 60.59 % after four cycles. This reduction in adsorption efficiency of 2 % NaOH-BC for Pb^{2+} ions could be due to the partial destruction of active sites and mass loss during desorption.

3.3.6. *Adsorption mechanism of Pb^{2+} on alkaline biochar*

Ion exchange, complexation, and electrostatic interactions are reported as the primary mechanisms for Pb removal (Kołodyńska et al.,

2012; Li et al., 2017). However, the dominant mechanism depends on the biochar's properties, which are influenced by factors such as feedstock type, pyrolysis temperature, and solution pH.

Based on kinetics and isotherm studies, Pb^{2+} removal from alkaline biochars primarily occurred through chemisorption, resulting in monolayer adsorption on thesurface. This confirms that Pb^{2+} was adsorbed onto well-defined active sites on the alkaline biochar surface rather than through multilayer coverage. Electrostatic interactions also played a role in Pb^{2+} adsorption, influenced by pH-dependent surface charge effects. At higher pH levels, deprotonation of functional groups ($–COO^-$, $–O^-$) increased the negative surface charge, enhancing Pb^{2+} binding through electrostatic attraction. This aligns with the observed trend of increasing adsorption efficiency at higher pH, as shown in Fig. 6**b**.

XPS analysis further provided direct evidence of Pb^{2+} binding onto 2 % NaOH-BC. As shown in Fig. 7**a**, the full-range spectra after adsorption clearly revealed the emergence of Pb signals, indicating successful Pb uptake by 2 % NaOH-BC. The deconvoluted Pb 4f spectrum displayed two distinct peaks at 138.5 eV (Pb 4f 7/2) and 143.4 eV (Pb 4f 5/2) (Fig. 7**b**) (Fen et al., 2013). In the C 1s spectra, the C—C/C═C peak (284.0 eV) and the C═O peak (288.5 eV) shifted to 284.6 eV and 288.1 eV, respectively, after Pb^{2+} adsorption (Fig. 7**c**), reflecting changes in the electronic environment (Liu et al., 2020; Zhou et al., 2018). Additionally, the significant reduction in the C═O peak area after Pb^{2+} adsorption suggests its involvement, likely through coordination via Pb-O bonds (Junjie Zhang et al., 2019). The deconvoluted O 1s spectra further supported these findings. As depicted in Fig. 7d, the peak at ~531.2 eV, associated with carbonyl oxygen (C═O), shifted slightly to ~531.1 eV after adsorption, with an increase in intensity and area. This indicates the potential formation of Pb-O bonds, confirming the active role of carbonyl groups in Pb^{2+} binding (Chen et al., 2019; Zama et al., 2017). Furthermore, the peak at 532.4 eV, corresponding to oxygen in hydroxyl (C–OH) and/or carboxylate ($–COO^-$) groups, remained largely unchanged in position but exhibited a slight reduction in intensity, suggesting limited involvement of these groups in Pb^{2+} adsorption. Additionally, the disappearance of Na 1s signals in the full XPS survey spectrum after Pb^{2+}adsorption further confirms that ion exchange played a significant role in the adsorption process, where Pb^{2+} ions replaced Na^+ ions originally present on the biochar surface. In summary, our results indicated that Pb^{2+} ions were strongly adsorbed onto NaOH-modified biochar mainly through electrostatic interactions, ion exchange, and complexation.

3.3.7. *Practical considerations for large-scale application*

While the adsorption efficiency and reusability of NaOH-modified biochar were demonstrated under laboratory conditions, large-scale implementation requires further evaluation. The dry impregnation method in this study offers advantages such as reduced chemical

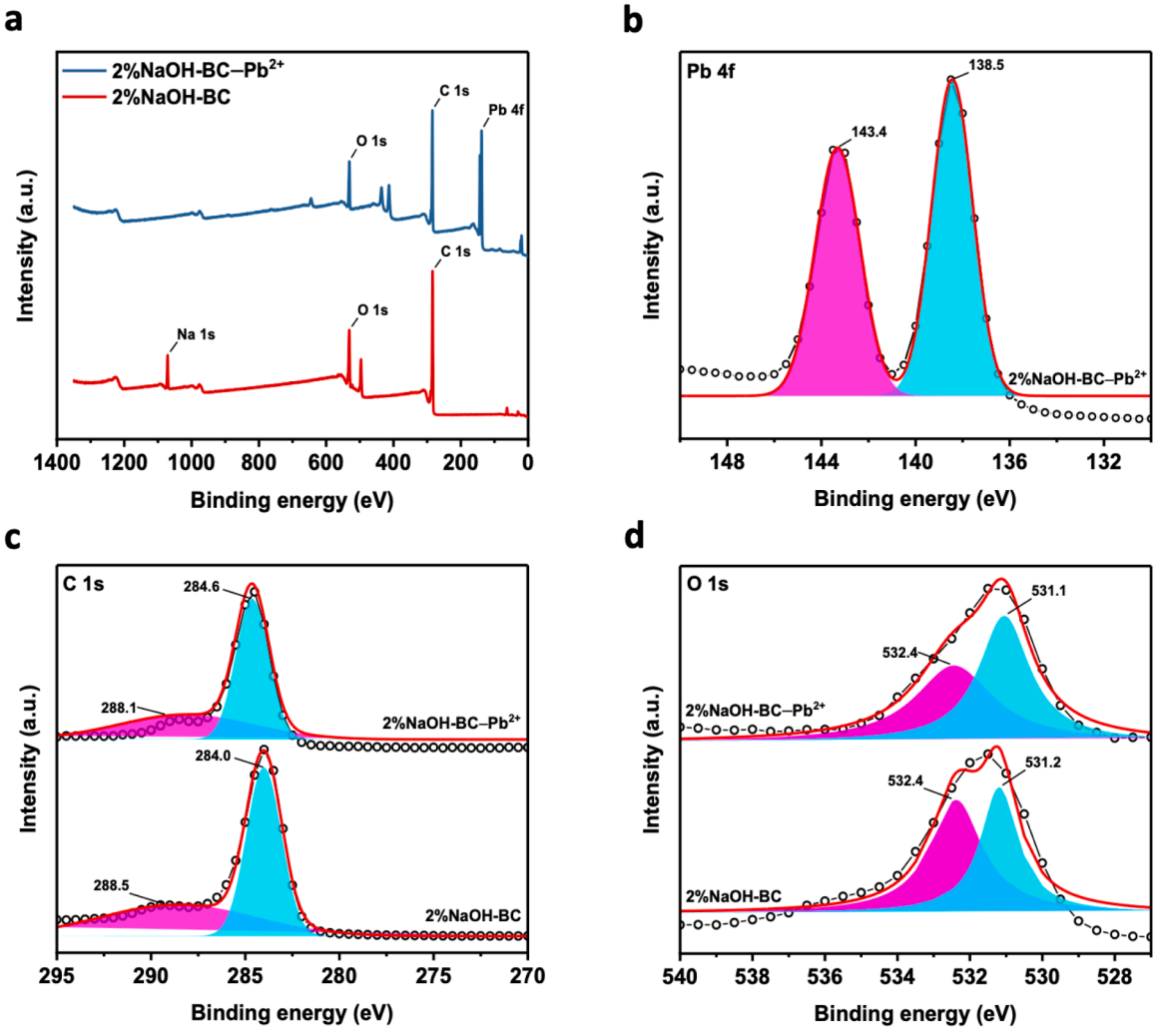

Fig. 7. XPS spectra of 2 % NaOH-BC: (**a**) Full-survey scan before (red curve) and after (blue curve) Pb^{2+}adsorption, (**b**) Pb 4f spectrum after Pb^{2+} adsorption, (**c**) C 1s spectra, and (**d**) O 1s spectra, both before and after Pb^{2+}adsorption.

consumption and miminized liquid waste generation, making it more cost-effective and environmentally sustainable than conventional alkaline treatments. For mass production of biochar, the aspects including feedstock availability, energy consumption, and maintaining consistent performance across diverse environmental conditions should be taken into consideration (Ambaye et al., 2021). Recyclability and regeneration are also important for practical applications. Optimizing separation and regeneration methods is essential to maintaining adsorption performance over multiple cycles. Structured biochar forms, such as pellets, granules, or magnetic composites, could improve handling and recovery. Moreover, real-world applications must account for competitive adsorption in complex matrices with multiple contaminants, which may influence Pb^{2+} removal. Further studies should focus on pilot-scale evaluations, economic feasibility assessments, and life-cycle analyses to determine the practicality and long-term sustainability of NaOH-modified biochar for heavy metal remediation.

4. Conclusions

This study demonstrated the high efficiency of alkaline biochar derived from pine wood in Pb^{2+} removal, with the 2 % NaOH-treated biochar achieving an adsorption capacity of 230 mg g^{-1}, far exceeding the non-alkaline biochar. Kinetic studies indicated that the adsorption process was dominated by chemisorption, as described by the pseudo-second-order model, while the Langmuir isotherm provided the best fit (R^2 = 0.933–0.970), confirming monolayer adsorption. The adsorption performance was strongly influenced by pH, with alkaline conditions enhancing Pb^{2+} uptake due to increased surface deprotonation and availability of negatively charged functional groups. XPS analysis supported these findings by revealing interactions between Pb^{2+} and oxygen-containing functional groups, particularly C═O, as evidenced by shifts in binding energies and changes in peak intensities. The absence of Na signals after Pb^{2+} adsorption further confirmed that ion exchange played a significant role in the removal mechanism, alongside electrostatic interactions and coordination with oxygen-containing functional groups. The recyclability of the alkaline biochar was validated through adsorption-desorption studies, demonstrating its practicality for repeated use. These findings underscore the potential of alkaline biochar for efficient Pb^{2+} removal and broader applications in environmental remediation.

Funding

This work was supported by the USDA Forest Service (Grant No 23-JV-11111124-053 and 24-JV-11111124-017).

CRediT authorship contribution statement

Qiangu Yan: Writing – original draft, Writing – review & editing, Methodology, Conceptualization, Investigation. **Neda Arabzadeh Nosratabad:** Writing – original draft, Writing – review & editing, Methodology, Investigation. **Xiangwei Du:** Formal analysis. **Timothy Ketelboeter:** Resources, Investigation, Writing – review & editing. **Caixia Wan:** Writing – review & editing, Supervision, Conceptualization, Funding acquisition, Project administration. **Zhiyong Cai:** Writing – review & editing, Supervision, Conceptualization, Funding acquisition, Project administration.

Declaration of competing interest

The authors declare that they have no known competing financial interests or personal relationships that could have appeared to influence the work reported in this paper.

Acknowledgements

The authors thank the financial support from the USDA Forest Service (Grant No 23-JV-11111124–053 and 24-JV-11111124–017).

Supplementary materials

Supplementary material associated with this article can be found, in the online version, at doi:10.1016/j.hazadv.2025.100657.

Data availability

Data will be made available on request.

References

Ahmad, Z., Gao, B., Mosa, A., Yu, H., Yin, X., Bashir, A., Ghoveisi, H., Wang, S., 2018. Removal of Cu(II), Cd(II) and Pb(II) ions from aqueous solutions by biochars derived from potassium-rich biomass. J. Clean. Prod. 180, 437–449. https://doi.org/10.1016/j.jclepro.2018.01.133.

Al-Ghouti, M.A., Li, J., Salamh, Y., Al-Laqtah, N., Walker, G., Ahmad, M.N.M., 2010. Adsorption mechanisms of removing heavy metals and dyes from aqueous solution using date pits solid adsorbent. J. Hazard. Mater. 176, 510–520. https://doi.org/10.1016/j.jhazmat.2009.11.059.

Amalina, F., Krishnan, S., Zularisam, A.W., Nasrullah, M., 2024. Pristine and modified biochar applications as multifunctional component towards sustainable future: recent advances and new insights. Sci. Total Environ. 914, 169608. https://doi.org/10.1016/j.scitotenv.2023.169608.

Ambaye, T., Vaccari, M., van Hullebusch, E.D., Amrane, A., Rtimi, S., 2021. Mechanisms and adsorption capacities of biochar for the removal of organic and inorganic pollutants from industrial wastewater. Int. J. Environ. Sci. Technol. 18 (10), 3273–3294. https://doi.org/10.1007/s13762-020-03060-w.

Amin, M., Alazba, A., Shafiq, M., 2018. Removal of copper and lead using banana biochar in batch adsorption systems: isotherms and kinetic studies. Arab. J. Sci. Eng. 43, 5711–5722. https://doi.org/10.1007/s13369-017-2934-z.

Amosa, M.K., 2016. Sorption of water alkalinity and hardness from high-strength wastewater on bifunctional activated carbon: process optimization, kinetics and equilibrium studies. Environ. Technol. 37, 2016–2039. https://doi.org/10.1080/09593330.2016.1139631.

Bashir, S., Zhu, J., Fu, Q., Hu, H., 2018. Comparing the adsorption mechanism of Cd by rice straw pristine and KOH-modified biochar. Environ. Sci. Pollut. Res. Int. 25, 11875–11883. https://doi.org/10.1007/s11356-018-1292-z.

Bentley, M.J., Kearns, J.P., Murphy, B.M., Summers, R.S., 2022. Pre-pyrolysis metal and base addition catalyzes pore development and improves organic micropollutant adsorption to pine biochar. Chemosphere 286, 131949. https://doi.org/10.1016/j.chemosphere.2021.131949.

Cai, T., Du, H., Liu, X., Tie, B., Zeng, Z., 2021. Insights into the removal of Cd and Pb from aqueous solutions by NaOH–EtOH-modified biochar. Environ. Technol. Innov. 24, 102031. https://doi.org/10.1016/j.eti.2021.102031.

Carrier, M., Loppinet-Serani, A., Denux, D., Lasnier, J.-M., Ham-Pichavant, F., Cansell, F., Aymonier, C., 2011. Thermogravimetric analysis as a new method to determine the lignocellulosic composition of biomass. Biomass Bioenergy 35, 298–307. https://doi.org/10.1016/j.biombioe.2010.08.067.

Cazetta, A.L., Vargas, A.M., Nogami, E.M., Kunita, M.H., Guilherme, M.R., Martins, A.C., Silva, T.L., Moraes, J.C., Almeida, V.C., 2011. NaOH-activated carbon of high surface area produced from coconut shell: kinetics and equilibrium studies from the methylene blue adsorption. Chem. Eng. J. 174, 117–125. https://doi.org/10.1016/j.cej.2011.08.058.

Chandraiah, M.R., 2016. Facile synthesis of zero valent iron magnetic biochar composites for Pb (II) removal from the aqueous medium. Alexandria Eng. J. 55, 619–625. https://doi.org/10.1016/j.aej.2015.12.015.

Chen, W., Lu, Z., Xiao, B., Gu, P., Yao, W., Xing, J., Asiri, A.M., Alamry, K.A., Wang, X., Wang, S., 2019a. Enhanced removal of lead ions from aqueous solution by iron oxide nanomaterials with cobalt and nickel doping. J. Clean. Prod. 211, 1250–1258. https://doi.org/10.1016/j.jclepro.2018.11.254.

Chen, W., Yang, H., Chen, Y., Chen, X., Fang, Y., Chen, H., 2016. Biomass pyrolysis for nitrogen-containing liquid chemicals and nitrogen-doped carbon materials. J. Anal. Appl. Pyrolysis 120, 186–193. https://doi.org/10.1016/j.jaap.2016.05.004.

Chen, Z.-l., Zhang, J.-q., Huang, L., Yuan, Z.-h., Li, Z.-j., Liu, M.-c, 2019b. Removal of Cd and Pb with biochar made from dairy manure at low temperature. J. Integr. Agric. 18, 201–210. https://doi.org/10.1016/S2095-3119(18)61987-2.

Ding, Y., Liu, Y., Liu, S., Li, Z., Tan, X., Huang, X., Zeng, G., Zhou, Y., Zheng, B., Cai, X., 2016. Competitive removal of Cd (II) and Pb (II) by biochars produced from water hyacinths: performance and mechanism. RSC Adv 6, 5223–5232. https://doi.org/10.1039/C5RA26248H.

Fen, Y.W., Yunus, W.M.M., Talib, Z.A., 2013. Analysis of Pb (II) ion sensing by crosslinked chitosan thin film using surface plasmon resonance spectroscopy. Optik (Stuttg) 124, 126–133. https://doi.org/10.1016/j.ijleo.2011.11.035.

Freundlich, H., 1907. Over the adsorption in solution. J. Phys. Chem. B 57, 385–470. https://doi.org/10.1515/zpch-1907-5723.

Fu, F., Wang, Q., 2011. Removal of heavy metal ions from wastewaters: a review. J. Environ. Manage. 92, 407–418. https://doi.org/10.1016/j.jenvman.2010.11.011.
Fytianos, K., Voudrias, E., Kokkalis, E., 2000. Sorption–desorption behaviour of 2,4-dichlorophenol by marine sediments. Chemosphere 40, 3–6. https://doi.org/10.1016/S0045-6535(99)00214-3.
Genç-Fuhrman, H., Mikkelsen, P.S., Ledin, A., 2016. Simultaneous removal of As, Cd, Cr, Cu, Ni and Zn from stormwater using high-efficiency industrial sorbents: effect of pH, contact time and humic acid. Sci. Total Environ. 566, 76–85. https://doi.org/10.1016/j.scitotenv.2016.04.210.
Gupta, N.K., Prakash, P., Kalaichelvi, P., Sheeba, K., 2016. The effect of temperature and hemicellulose-lignin, cellulose-lignin, and cellulose-hemicellulose on char yield from the slow pyrolysis of rice husk. Energy Sources Part A 38, 1428–1434. https://doi.org/10.1080/15567036.2014.941518.
Hagemann, N., Spokas, K., Schmidt, H.-P., Kägi, R., Böhler, M.A., Bucheli, T.D., 2018. Activated carbon, biochar and charcoal: linkages and synergies across pyrogenic carbon's ABC s. Water (Basel) 10, 182. https://doi.org/10.3390/w10020182.
Hameed, B.H., Tan, I.A.W., Ahmad, A.L., 2008. Adsorption isotherm, kinetic modeling and mechanism of 2,4,6-trichlorophenol on coconut husk-based activated carbon. Chem. Eng. J. 144, 235–244. https://doi.org/10.1016/j.cej.2008.01.028.
Ippolito, J., Strawn, D., Scheckel, K., Novak, J., Ahmedna, M., Niandou, M., 2012. Macroscopic and molecular investigations of copper sorption by a steam-activated biochar. J. Environ. Qual. 41, 1150–1156. https://doi.org/10.2134/jeq2011.0113.
Ippolito, J.A., Cui, L., Kammann, C., Wrage-Mönnig, N., Estavillo, J.M., Fuertes-Mendizabal, T., Cayuela, M.L., Sigua, G., Novak, J., Spokas, K., Borchard, N., 2020. Feedstock choice, pyrolysis temperature and type influence biochar characteristics: a comprehensive meta-data analysis review. Biochar 2, 421–438. https://doi.org/10.1007/s42773-020-00067-x.
Jin, H., Capareda, S., Chang, Z., Gao, J., Xu, Y., Zhang, J., 2014. Biochar pyrolytically produced from municipal solid wastes for aqueous As(V) removal: adsorption property and its improvement with KOH activation. Bioresour. Technol. 169, 622–629. https://doi.org/10.1016/j.biortech.2014.06.103.
Keiluweit, M., Nico, P.S., Johnson, M.G., Kleber, M., 2010. Dynamic molecular structure of plant biomass-derived black carbon (Biochar). J. Environ. Sci. Technol. 44, 1247–1253. https://doi.org/10.1021/es9031419.
Kołodyńska, D., Wnętrzak, R., Leahy, J., Hayes, M., Kwapiński, W., Hubicki, Z., 2012. Kinetic and adsorptive characterization of biochar in metal ions removal. Chem. Eng. J. 197, 295–305. https://doi.org/10.1016/j.cej.2012.05.025.
Kwak, J.-H., Islam, M.S., Wang, S., Messele, S.A., Naeth, M.A., El-Din, M.G., Chang, S.X., 2019. Biochar properties and lead(II) adsorption capacity depend on feedstock type, pyrolysis temperature, and steam activation. Chemosphere 231, 393–404. https://doi.org/10.1016/j.chemosphere.2019.05.128.
Langmuir, I., 1918. The adsorption of gases on plane surfaces of glass, mica and platinum. J. Am. Chem. Soc. 40, 1361–1403. https://doi.org/10.1021/ja02242a004.
Lee, H.-S., Shin, H.-S., 2021. Competitive adsorption of heavy metals onto modified biochars: comparison of biochar properties and modification methods. J. Environ. Manage. 299, 113651. https://doi.org/10.1016/j.jenvman.2021.113651.
Li, H., Dong, X., da Silva, E.B., de Oliveira, L.M., Chen, Y., Ma, L.Q., 2017. Mechanisms of metal sorption by biochars: biochar characteristics and modifications. Chemosphere 178, 466–478. https://doi.org/10.1016/j.chemosphere.2017.03.072.
Liu, J., Huang, Z., Chen, Z., Sun, J., Gao, Y., Wu, E., 2020. Resource utilization of swine sludge to prepare modified biochar adsorbent for the efficient removal of Pb(II) from water. J. Clean. Prod. 257, 120322. https://doi.org/10.1016/j.jclepro.2020.120322.
Liu, P., Liu, W.-J., Jiang, H., Chen, J.-J., Li, W.-W., Yu, H.-Q., 2012. Modification of biochar derived from fast pyrolysis of biomass and its application in removal of tetracycline from aqueous solution. Bioresour. Technol. 121, 235–240. https://doi.org/10.1016/j.biortech.2012.06.085.
Liu, W.-J., Li, W.-W., Jiang, H., Yu, H.-Q., 2017. Fates of chemical elements in biomass during its pyrolysis. Chem. Rev. 117, 6367–6398. https://doi.org/10.1021/acs.chemrev.6b00647.
Liu, Z., Xu, Z., Xu, L., Buyong, F., Chay, T.C., Li, Z., Cai, Y., Hu, B., Zhu, Y., Wang, X., 2022. Modified biochar: synthesis and mechanism for removal of environmental heavy metals. Carbon Res 1, 8. https://doi.org/10.1007/s44246-022-00007-3.
Liu, Z., Zhang, F.-S., 2009. Removal of lead from water using biochars prepared from hydrothermal liquefaction of biomass. J. Hazard. Mater. 167, 933–939. https://doi.org/10.1016/j.jhazmat.2009.01.085.
Lu, K., Yang, X., Gielen, G., Bolan, N., Ok, Y.S., Niazi, N.K., Xu, S., Yuan, G., Chen, X., Zhang, X., 2017. Effect of bamboo and rice straw biochars on the mobility and redistribution of heavy metals (Cd, Cu, Pb and Zn) in contaminated soil. J. Environ. Manage. 186, 285–292. https://doi.org/10.1016/j.jenvman.2016.05.068.
Lu, L., Kong, C., Sahajwalla, V., Harris, D., 2002. Char structural ordering during pyrolysis and combustion and its influence on char reactivity. Fuel 81, 1215–1225. https://doi.org/10.1016/S0016-2361(02)00035-2.
Mahdi, Z., El Hanandeh, A., Yu, Q.J., 2019. Preparation, characterization and application of surface modified biochar from date seed for improved lead, copper, and nickel removal from aqueous solutions. J. Environ. Chem. Eng. 7, 103379. https://doi.org/10.1016/j.jece.2019.103379.
Mohan, D., Kumar, H., Sarswat, A., Alexandre-Franco, M., Pittman Jr, C.U., 2014. Cadmium and lead remediation using magnetic oak wood and oak bark fast pyrolysis bio-chars. Chem. Eng. J. 236, 513–528. https://doi.org/10.1016/j.cej.2013.09.057.
Monga, D., Shetti, N.P., Basu, S., Raghava Reddy, K., Badawi, M., Bonilla-Petriciolet, A., Aminabhavi, T.M., 2022. Engineered biochar: a way forward to environmental remediation. Fuel 311, 122510. https://doi.org/10.1016/j.fuel.2021.122510.
Murtaza, G., Ahmed, Z., Valipour, M., Ali, I., Usman, M., Iqbal, R., Zulfiqar, U., Rizwan, M., Mahmood, S., Ullah, A., 2024. Recent trends and economic significance of modified/functionalized biochars for remediation of environmental pollutants. Sci. Rep. 14, 217. https://doi.org/10.1038/s41598-023-50623-1.
Namazian, M., Halvani, S., 2006. Calculations of pKa values of carboxylic acids in aqueous solution using density functional theory. J. Chem. Thermodyn. 38, 1495–1502. https://doi.org/10.1016/j.jct.2006.05.002.
Nguyen, V.-T., Nguyen, T.-B., Chen, C.-W., Hung, C.-M., Huang, C., Dong, C.-D., 2019. Cobalt-impregnated biochar (Co-SCG) for heterogeneous activation of peroxymonosulfate for removal of tetracycline in water. Bioresour. Technol. 292, 121954. https://doi.org/10.1016/j.biortech.2019.121954.
Nosratabad, N.A., Yan, Q., Cai, Z., Wan, C., 2024. Exploring nanomaterial-modified biochar for environmental remediation applications. Heliyon 10, e37123. https://doi.org/10.1016/j.heliyon.2024.e37123.
O'Connell, D.W., Birkinshaw, C., O'Dwyer, T.F, 2008. Heavy metal adsorbents prepared from the modification of cellulose: a review. Bioresour. Technol. 99, 6709–6724. https://doi.org/10.1016/j.biortech.2008.01.036.
Omidi, A.H., Cheraghi, M., Lorestani, B., Sobhanardakani, S., Jafari, A., 2019. Biochar obtained from cinnamon and cannabis as effective adsorbents for removal of lead ions from water. Environ. Sci. Pollut. Res. 26, 27905–27914. https://doi.org/10.1007/s11356-019-05997-z.
Omidvar-Hosseini, F., Moeinpour, F., 2016. Removal of Pb (II) from aqueous solutions using acacia nilotica seed shell ash supported Ni0. 5Zn0. 5Fe2O4 magnetic nanoparticles. J. Water Reuse Desalin. 6, 562–573. https://doi.org/10.2166/wrd.2016.073.
Ramola, S., Mohan, D., Masek, O., Méndez, A., Tsubota, T., 2022. Engineered Biochar: Fundamentals, Preparation, Characterization and Applications, 381. Springer.
Rizwan, M., Lin, Q., Chen, X., Li, Y., Li, G., Zhao, X., Tian, Y., 2020. Synthesis, characterization and application of magnetic and acid modified biochars following alkaline pretreatment of rice and cotton straws. Sci. Total Environ. 714, 136532. https://doi.org/10.1016/j.scitotenv.2020.136532.
Shin, J., Lee, Y.-G., Lee, S.-H., Kim, S., Ochir, D., Park, Y., Kim, J., Chon, K., 2020. Single and competitive adsorptions of micropollutants using pristine and alkali-modified biochars from spent coffee grounds. J. Hazard. Mater. 400, 123102. https://doi.org/10.1016/j.jhazmat.2020.123102.
Sugama, T., Pyatina, T., 2015. Effect of sodium carboxymethyl celluloses on water-catalyzed self-degradation of 200 C-heated alkali-activated cement. Cem. Concr. Compos. 55, 281–289. https://doi.org/10.1016/j.cemconcomp.2014.09.015.
Tan, I., Ahmad, A.L., Hameed, B., 2008. Adsorption of basic dye on high-surface-area activated carbon prepared from coconut husk: equilibrium, kinetic and thermodynamic studies. J. Hazard. Mater. 154, 337–346. https://doi.org/10.1016/j.jhazmat.2007.10.031.
Tomczyk, A., Sokołowska, Z., Boguta, P., 2020. Biochar physicochemical properties: pyrolysis temperature and feedstock kind effects. Rev. Environ. Sci. Biotechnol. 19, 191–215. https://doi.org/10.1007/s11157-020-09523-3.
Uchimiya, M., Bannon, D.I., Wartelle, L.H., Lima, I.M., Klasson, K.T., 2012. Lead retention by broiler litter biochars in small arms range soil: impact of pyrolysis temperature. J. Agric. Food. Chem. 60, 5035–5044. https://doi.org/10.1021/jf300825n.
Vijayaraghavan, K., Padmesh, T.V.N., Palanivelu, K., Velan, M., 2006. Biosorption of nickel(II) ions onto Sargassum wightii: application of two-parameter and three-parameter isotherm models. J. Hazard. Mater. 133, 304–308. https://doi.org/10.1016/j.jhazmat.2005.10.016.
Wang, C., Wang, H., Cao, Y., 2018. Pb (II) sorption by biochar derived from Cinnamomum camphora and its improvement with ultrasound-assisted alkali activation. Colloids Surf. A: Physicochem. Eng. Asp. 556, 177–184. https://doi.org/10.1016/j.colsurfa.2018.08.036.
Wang, J., Wang, S., 2019. Preparation, modification and environmental application of biochar: a review. J. Clean. Prod. 227, 1002–1022. https://doi.org/10.1016/j.jclepro.2019.04.282.
Weber, T.W., Chakravorti, R.K., 1974. Pore and solid diffusion models for fixed-bed adsorbers. AIChE J 20, 228–238. https://doi.org/10.1002/aic.690200204.
Wu, Q., Xian, Y., He, Z., Zhang, Q., Wu, J., Yang, G., Zhang, X., Qi, H., Ma, J., Xiao, Y., 2019. Adsorption characteristics of Pb (II) using biochar derived from spent mushroom substrate. Sci. Rep. 9, 15999. https://doi.org/10.1038/s41598-019-52554-2.
Xu, X., Cao, X., Zhao, L., Wang, H., Yu, H., Gao, B., 2013. Removal of Cu, Zn, and Cd from aqueous solutions by the dairy manure-derived biochar. Environ. Sci. Pollut. Res. 20, 358–368. https://doi.org/10.1007/s11356-012-0873-5.
Yang, F., Zhang, S., Cho, D.-W., Du, Q., Song, J., Tsang, D.C.W, 2019. Porous biochar composite assembled with ternary needle-like iron-manganese-sulphur hybrids for high-efficiency lead removal. Bioresour. Technol. 272, 415–420. https://doi.org/10.1016/j.biortech.2018.10.068.
Yap, M., Mubarak, N., Sahu, J., Abdullah, E., 2017. Microwave induced synthesis of magnetic biochar from agricultural biomass for removal of lead and cadmium from wastewater. J. Ind. Eng. Chem. 45, 287–295. https://doi.org/10.1016/j.jiec.2016.09.036.
Yari, M., Rajabi, M., Moradi, O., Yari, A., Asif, M., Agarwal, S., Gupta, V.K., 2015. Kinetics of the adsorption of Pb (II) ions from aqueous solutions by graphene oxide and thiol functionalized graphene oxide. J. Mol. Liq. 209, 50–57. https://doi.org/10.1016/j.molliq.2015.05.022.
Zahedifar, M., Seyedi, N., Shafiei, S., Basij, M., 2021. Surface-modified magnetic biochar: highly efficient adsorbents for removal of Pb (II) and Cd (II). Mater. Chem. Phys. 271, 124860. https://doi.org/10.1016/j.matchemphys.2021.124860.
Zama, E.F., Zhu, Y.-G., Reid, B.J., Sun, G.-X., 2017. The role of biochar properties in influencing the sorption and desorption of Pb(II), Cd(II) and As(III) in aqueous solution. J. Clean. Prod. 148, 127–136. https://doi.org/10.1016/j.jclepro.2017.01.125.
Zhang, J., Huang, B., Chen, L., Du, J., Li, W., Luo, Z., 2018. Pyrolysis kinetics of hulless barley straw using the distributed activation energy model (DAEM) by the TG/DTA

technique and SEM/XRD characterizations for hulless barley straw derived biochar. Braz. J. Chem. Eng. 35, 1039–1050. https://doi.org/10.1590/0104-6632.20180353s20170382.

Zhang, J., Shao, J., Jin, Q., Li, Z., Zhang, X., Chen, Y., Zhang, S., Chen, H., 2019. Sludge-based biochar activation to enhance Pb (II) adsorption. Fuel 252, 101–108. https://doi.org/10.1016/j.fuel.2019.04.096.

Zhao, J., Ye, Z.-L., Pan, X., Cai, G., Wang, J., 2022. Screening the functions of modified rice straw biochar for adsorbing manganese from drinking water. RSC Adv 12, 15222–15230. https://doi.org/10.1039/D2RA01720B.

Zhou, N., Chen, H., Xi, J., Yao, D., Zhou, Z., Tian, Y., Lu, X., 2017. Biochars with excellent Pb(II) adsorption property produced from fresh and dehydrated banana peels via hydrothermal carbonization. Bioresour. Technol. 232, 204–210. https://doi.org/10.1016/j.biortech.2017.01.074.

Zhou, X., Liu, Y., Zhou, J., Guo, J., Ren, J., Zhou, F., 2018. Efficient removal of lead from aqueous solution by urea-functionalized magnetic biochar: preparation, characterization and mechanism study. J. Taiwan Inst. Chem. Eng. 91, 457–467. https://doi.org/10.1016/j.jtice.2018.04.018.